Available online at www.sciencedirect.com
SCIENCE DIRECT®
Journal of Power Sources 134 (2004) 33–40
JOURNAL OF POWER SOURCES
www.elsevier.com/locate/jpowsour

Electrochemical and flow characterization of a direct methanol fuel cell

G.Q. Lu, C.Y. Wang*

Electrochemical Engine Center (ECEC), Department of Mechanical and Nuclear Engineering, The Pennsylvania State University, University Park, PA 16802, USA

Received 7 January 2004; accepted 30 January 2004

Available online 18 May 2004

Abstract

Two-phase phenomena, i.e. bubble flow in the anode and water flooding in the cathode, are critical to design of high-performance direct methanol fuel cells (DMFC). A 5 cm^2 transparent DMFC has been developed to visualize these phenomena in situ. Two types of membrane-electrode assembly (MEA) based on Nafion® 112 were used to investigate effects of backing pore structure and wettability on cell polarization characteristics and two-phase flow dynamics. One employed carbon paper backing material and the other carbon cloth. Experiments were performed under conditions of various methanol feed concentrations. The transparent fuel cell was shown to reach a peak power of 93 mW/cm^2 at 0.3 V, using Toray carbon-paper based MEA under 2 M methanol solution preheated at 85 °C. For the hydrophobic carbon paper backing, it was observed that CO_2 bubbles nucleate at certain locations and form large and discrete bubble slugs in the channel. For the hydrophilic carbon cloth backing, it was shown that bubbles are produced more uniformly and of smaller size. It is thus shown that the anode backing layer of uniform pore size and more hydrophilicity is preferred for gas management in the anode. Flow visualization of water flooding on the cathode side of DMFC has also been carried out. It is shown that liquid droplets appear more easily on the surface of carbon paper due to its reduced hydrophobicity at elevated temperature. For the single-side ELAT carbon cloth, liquid droplets tend to form in the corner between the current collecting rib and GDL since ELAT is highly hydrophobic and the rib (stainless steel) surface is hydrophilic.

Keywords: Direct methanol fuel cell; Methanol crossover; CO_2 bubble dynamics; Cathode flooding; Two-phase flow; GDL wettability; Flow visualization

1. Introduction

The direct methanol fuel cell (DMFC) has attracted much attention due to its potential applications as a power source for transportation and portable electronic devices [1–8]. Lamy et al. [9] and Arico et al. [10] have provided the most recent reviews of the DMFC system. Among critical problems remaining to be solved in the improvement of the DMFC performance are slow anode kinetics, methanol crossover through the polymer electrolyte, gas management on the anode, and water management on the cathode. The deleterious methanol crossover from anode to cathode significantly reduces open circuit voltage as well as fuel efficiency. Narayanan et al. [1] reported the influence of the Nafion® membrane thickness on methanol crossover rate. Valdez and Narayanan [11] found methanol crossover affected by temperature and indicated the crossover effect increased with cell temperature. Heinzel and Barragan [12] gave an extensive review of methanol crossover in direct methanol fuel cells, enumerating various parameters influencing methanol crossover, such as methanol concentration, pressure, temperature, membrane thickness, and catalyst morphology. Ren et al. [13] used lower methanol concentrations and optimized cell design to decrease methanol crossover in their fuel cell systems. Gurau and Smotkin [6] extensively characterized methanol crossover by gas chromatography. However, few papers considered the possibility of reducing methanol crossover by mass transport control in the backing layer and hence control of methanol feed rate.

Gas management on the anode side is an important issue in DMFC design. On the anode side, carbon dioxide is produced as a result of methanol electrochemical oxidation. If CO_2 bubbles cannot be removed efficiently, the anode channels will be blocked, leading to limited mass transport. Argyropoulos et al. [14,15] was perhaps among the first to observe the two-phase flow pattern in the anode channel under various operating conditions. This flow visualization

* Corresponding author. Tel.: +1-814-863-4762; fax: +1-814-863-4848.
E-mail address: cxw31@psu.edu (C.Y. Wang).

0378-7753/$ – see front matter © 2004 Elsevier B.V. All rights reserved.
doi:10.1016/j.jpowsour.2004.01.055

on the anode side yields valuable understanding of bubble dynamics in DMFC. This study was, however, undertaken under low cell performance; as such, the ensuing bubble dynamics may not be fully representative of those in a state-of-the-art DMFC. In addition, visualization resolution in Argyropoulos et al. [14,15] was somewhat inadequate, and no effect upon backing layer surface wettability was explored.

The importance of flooding on the cathode side in H_2/air polymer electrolyte fuel cells has been repeatedly emphasized in the literature [16,17]. Tuber et al. [18] most recently conducted a photographic study of two-phase flow and transport in a transparent H_2/air fuel cell, and presented images of liquid water distribution in the cathode gas channels to help understand electrode flooding. Similarly, water management on the cathode in the DMFC was identified as a key issue [8]. In the DMFC cathode, proper level of water concentration helps to humidify the polymer membrane. However, flooding occurs in the cathode if there is too much water, degrading the cathode performance significantly. In order to accurately predict critical operation conditions to avoid flooding, visualization on the cathode side is essential to yield fundamental physics behind the flooding occurrence.

The present work is concerned with simultaneous two-phase flow visualization and electrochemical characterization of the DMFC. A carefully designed transparent DMFC is developed to allow for visualization of both anode and cathode, in addition to cell performance characterization. Membrane-electrode assemblies (MEAs) with backing layers of differing wettability are used to explore the fundamental role of such wetting characteristics in DMFC. Polarization curves are measured at different methanol concentrations, with focus on revealing the relationship among the anode limiting current, methanol crossover rate, and anode backing structure. Flow visualization on the anode side is carried out to provide a fundamental understanding of bubble dynamics in DMFC and its controlling factors. Finally, cathode flooding is visualized, revealing a strong dependence on wettability of the cathode backing layer.

2. Experimental

2.1. Experimental rig and transparent cell design

Fig. 1 displays a diagram of the experimental setup, which consists of an electronic load system (BT4, Arbin) to characterize polarization behaviors of the fuel cell, a peristaltic pump to deliver the liquid fuel, an electric heater with temperature controller, pressure relief valves, flow meters and pressure gauges. Pressure relief valves were applied to control the back pressures at the exits of the anode and cathode. The electrical heater is a heat exchanger designed to preheat the methanol–water solution and air prior to flow through the fuel cell, with the temperature controlled at a prescribed value. No additional heater was used for the cell. A Sony digital video camera recorder was used in experiments for flow visualization, and still pictures can be captured according to the time sequence when the movie is edited offline. Also, a Nikon N70 camera with a microNikkor lens (60 mm f/2.8 D) was utilized to get clear pictures of small-size objects.

Fig. 2 shows a picture of the transparent fuel cell. The cell is constructed of a pair of a stainless steel plate mated with a polycarbonate plate. A total of eight (8) parallel flow channels (1.92 mm width, 1.5 mm depth, 1 mm rib width) were machined through the stainless steel plate to form an effective area of approximately 5 cm^2. The surface of the stainless steel plate contacting the MEA was coated with 30 nm Cr and 300 nm Au to minimize contact resistance. A

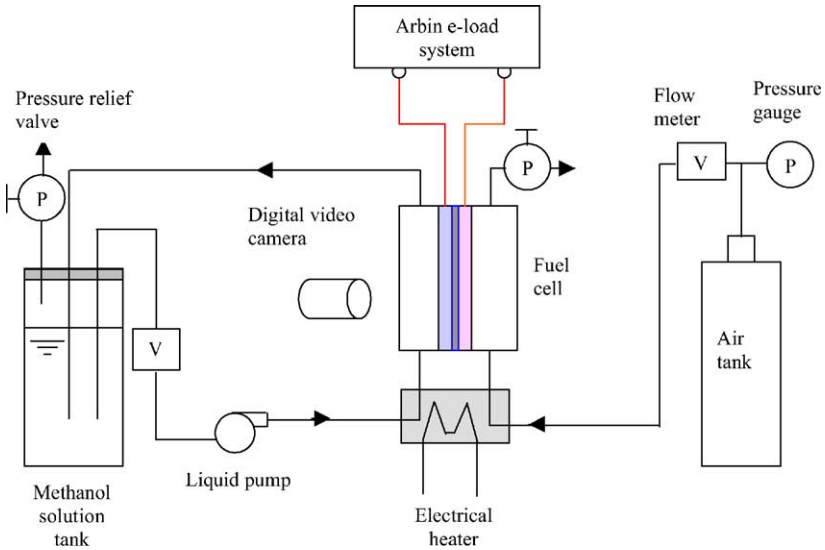

Fig. 1. Schematic of the experimental rig.

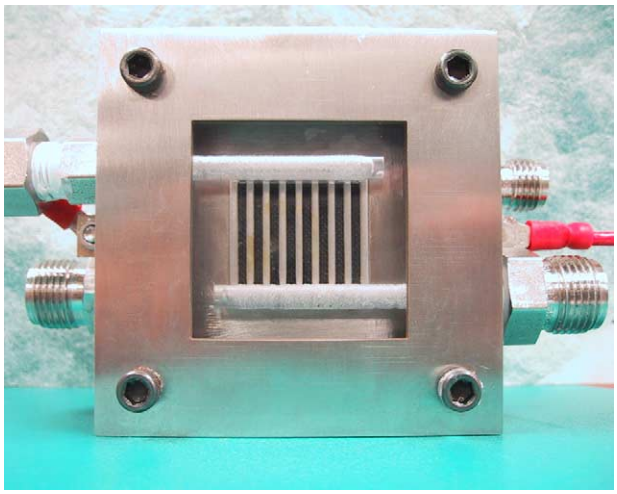

Fig. 2. Photo of the transparent fuel cell.

transparent polycarbonate plate covered the stainless steel plate, forming a window to allow direct observation of flow behaviors. The polycarbonate plate was concave in design, while the stainless steel plate had a matching convex pattern. This unique design avoided flow leakage between neighboring parallel channels. Cell inlet and outlet manifolds were also machined in the polycarbonate plates.

2.2. MEA Fabrication

In these experiments, two types of MEAs were used. One was fabricated in-house (dubbed ECEC MEA). Specifically, 20 wt.% FEP wet-proofed carbon paper (Toray 090, E-Tek) of 0.26 mm thickness was used as backing layer for both anode and cathode. A mixture solution containing Vulcan XC72R carbon black and 40 wt.% of Teflon (TFE 30, Dupont) was coated on the carbon paper to form a microporous layer with carbon loading of 2 mg/cm^2 and Teflon loading of 2 mg/cm^2. For the catalyst layer on the anode side, loadings of unsupported Pt/Ru black (HiSPEC 6000, Pt:Ru = 1:1 atomic ratio, Alfa Aesar) and Nafion® (EW1100, Aldrich) were 4 and 1 mg/cm^2, respectively. For the cathode catalyst layer, loadings of carbon-supported Pt (40 wt.% Pt on Vulcan XC72R, E-Tek) and Nafion® were 1.3 and 1 mg/cm^2, respectively. The catalyzed electrodes were hot-pressed to pretreated Nafion® 112 (EW 1100, Dupont) to make a MEA. More details on this MEA fabrication procedure have been given in Lim and Wang [19] and thus are not repeated here.

The other type of MEA used in this work was a commercially available MEA (C-MEA). This C-MEA has Pt/Ru loading of 4 mg/cm^2 on the anode side and untreated (thus hydrophilic) carbon cloth is used as the backing layer, while Pt loading of 4 mg/cm^2 on a single-sided ELAT carbon cloth is used for the cathode. In order to compare performance with the ECEC MEA, the C-MEA membrane was also Nafion® 112.

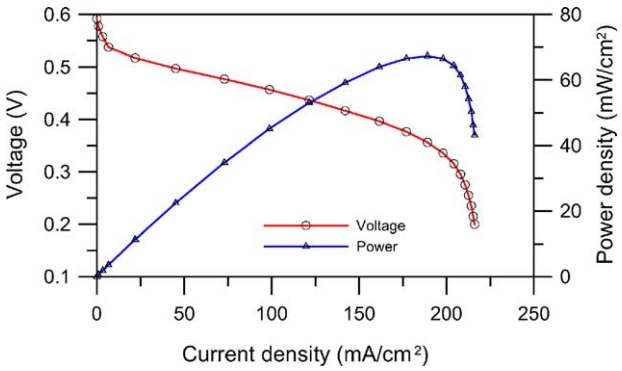

Fig. 3. Polarization and power density curves of the transparent cell using ECEC MEA (C paper) for 1 M MeOH feed (20.8 ml/min and 0 psig) and non-humidified air (700 ml/min and 15 psig) at 85 °C.

3. Results and discussion

3.1. Performance data

Polarization curves of the transparent fuel cell were measured extensively under different operation conditions. Fig. 3 shows the cell performance using the ECEC MEA. The operation conditions are 1 M methanol–water solution for the anode and non-humidified air at 15 psig for the cathode. Both fuel and air were preheated to 85 °C. The volume flow rates and backing pressures for the methanol and air are indicated in the figure. The maximum current density at the voltage of 0.2 V is 215 mA/cm^2, while the maximum power density is 69 mW/cm^2 at a voltage of 0.37 V. It should be noted that the cell itself could not be heated due to transparency required for visualization; therefore, actual cell temperature was about 10 °C lower than the feed stream temperature (i.e. 85 °C) due to heat loss from the cell to the surrounding environment.

Fig. 4 shows the performance of the transparent cell with ECEC MEA when 2 M methanol solution and non-humidified air were used under the same preheated temperature of 85 °C. When compared to the performance using 1 M methanol solution shown in Fig. 3, the open

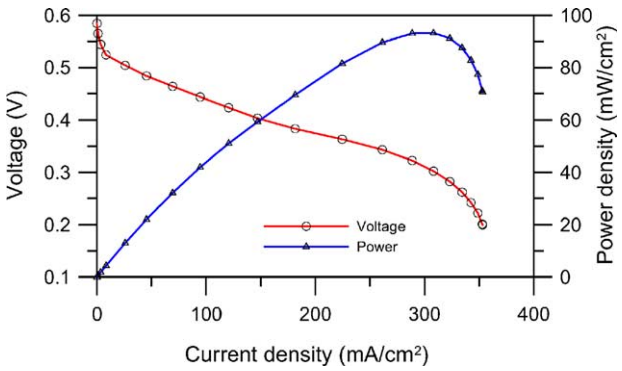

Fig. 4. Polarization and power density curves of the transparent cell using ECEC MEA (C paper) for 2 M MeOH feed (20.8 ml/min and 0 psig) and non-humidified air (700 ml/min and 15 psig) at 85 °C.

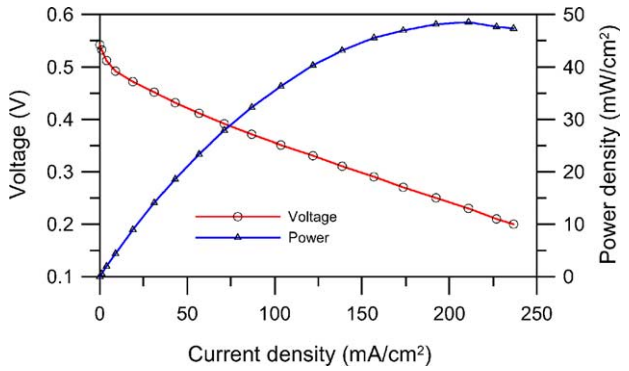

Fig. 5. Polarization and power density curves of the transparent cell using C-MEA (C cloth) for 1 M MeOH feed (20.8 ml/min and 0 psig) and non-humidified air (700 ml/min and 15 psig) at 85 °C.

circuit voltage with 2 M solution shown in Fig. 4 drops somewhat due to the stronger methanol crossover effect, although overall performance with 2 M solution increases substantially. As indicated in Fig. 4, the transparent fuel cell reaches a power output of 93 mW/cm^2 at 0.302 V. The cell with 2 M solution shows better performance than that with 1 M solution primarily due to mass transport limitation on the polarization curve.

Fig. 5 shows the performance of the transparent cell using the C-MEA with 1 M methanol solution and non-humidified air preheated to 85 °C. It can be seen from Fig. 5 that the maximum power density is below 48.5 mW/cm^2, slightly worse than the performance with the ECEC MEA (Fig. 3). It was found from more experiments (not shown here) that C-MEA performance declined even further with higher MeOH concentrations. Different anode backing structures cause ECEC MEA and C-MEA to respond differently to higher MeOH concentration (i.e. 2 M). C-MEA used a thinner and more porous backing layer of hydrophilic carbon cloth. However, ECEC MEA employed a thicker carbon paper coated with another compact microporous layer as the backing. Methanol crossover is therefore suppressed by lowering the methanol feed rate through the latter modified anode structure [19,20]. Such a strategy is an alternative to the development of novel or modified membranes to increase cell tolerance to high MeOH concentrations. Furthermore, blocking methanol transport through a resistive backing layer rather than a thicker membrane allows use of thin polymer membranes, thereby reducing ohmic loss in the cell. More results using concentrations much higher than 2 M have been shown by Lu et al. [20].

3.2. Visualization of CO_2 bubble dynamics on anode

The electrochemical reaction occuring on the DMFC anode is given by:

$$CH_3OH + H_2O \rightarrow CO_2 + 6H^+ + 6e^-$$

As can be seen, carbon dioxide gas is produced and must be removed from the backing layer by the anode flow. If CO_2 bubbles cannot be removed efficiently from the surface of the backing layer, they remain, covering the backing surface and hence decreasing the effective mass transfer area. In addition, flow blockage results, particularly in channels of small dimensions as required in microfuel cells or more compact portable fuel cells with the maximum volumetric power and energy densities.

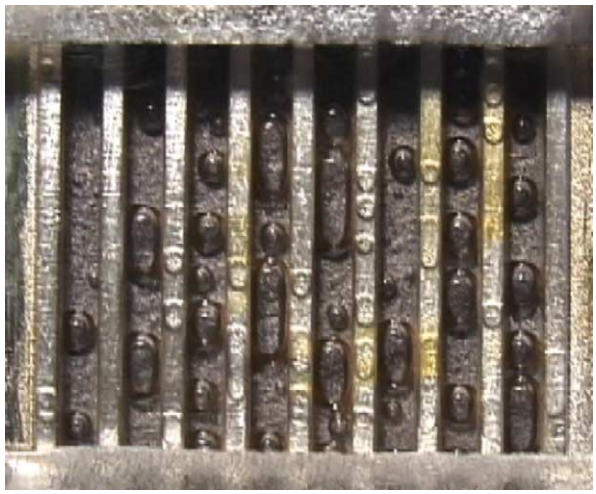

Fig. 6. Bubble behavior on the anode side using ECEC MEA (Hydrophobic carbon paper) for 2 M MeOH feed (20.8 ml/min and 0 psig) and non-humidified air (700 ml/min and 15 psig) at 40 mA/cm^2 and 85 °C.

Fig. 6 displays a raw image of bubbles using the ECEC MEA (with hydrophobic carbon paper as the backing layer) when the methanol solution and non-humidified air were preheated to 50 °C and the current density was fixed to 40 mA/cm^2. The image was captured from a movie recorded by a SONY digital video camera. As shown in Fig. 6, the CO_2 bubbles are large in size (~2 mm) and confined by channel dimensions, elongated in shape, and distributed discretely on the backing layer along the anode channel. This bubble flow is commonly categorized as Taylor bubbles.

Fig. 7 shows a sequence of images at various times for ECEC MEA at the feed temperature of 85 °C and the current density of 100 mA/cm^2. The images, one second apart, were captured from the movie, with time resolution 1/30 s. In addition, the time of the first image was chosen arbitrarily due to the fact that two-phase flow is a regularly periodic event. As shown in Fig. 7, the CO_2 bubbles nucleate at certain locations and form large and discrete gas slugs in the channel. The bubble motion is governed by the momentum of liquid flow, the force of buoyancy on the bubble, and the surface adhesion between bubbles and substrate. It can be seen from Fig. 7 that bubbles are held on the carbon paper by strong surface tension until they grow into larger slugs for detachment, clearly indicative of the dominant effect of surface tension in bubble dynamics in DMFC. Once the bubbles grow to a sufficient size, they detach and sweep along the backing surface in the channel. This sweeping process clears all small bubbles pre-existing on the backing surface, making new bubbles grow from the smallest size

Fig. 7. Images of bubble dynamics in the DMFC anode using ECEC MEA (carbon paper) for 2 M MeOH feed (20.8 ml/min and 0 psig) and non-humidified air (700 ml/min and 15 psig) at 100 mA/cm^2 and 85 °C.

to the full detachment diameter. As a result, the two-phase flow becomes regularly intermittent.

Fig. 8 shows the bubble patterns on C-MEA with hydrophilic carbon cloth also at the feed temperature of 85 °C. Since the carbon cloth has a much rougher surface, it is challenging to capture sharp still pictures due to light deflection, although the two-phase flow could be observed clearly in the experiments and movies. Alternatively, a Nikon N70 camera with a microNikkor lens was employed for still photos shown in Fig. 8. It is seen that the CO_2 bubbles are produced more uniformly and with smaller size (∼0.5 mm) from the hydrophilic carbon cloth.

The differences in bubble behaviors between hydrophobic carbon paper and hydrophilic carbon cloth can be explained by considering the fundamental process of bubble growth and detachment from pores of certain size and

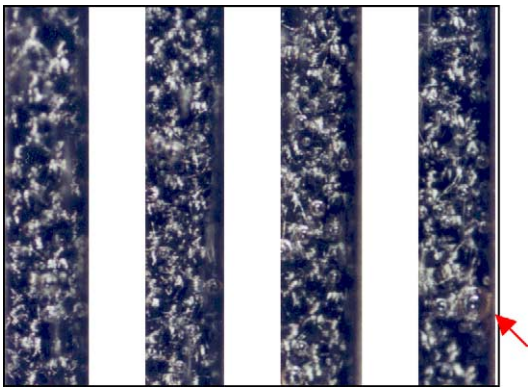

Fig. 8. Bubble behavior on the anode side using C-MEA (hydrophilic carbon cloth) for 1 M MeOH feed (20.8 ml/min and 0 psig) and non-humidified air (700 ml/min and 15 psig) at 100 mA/cm^2 and 85 °C.

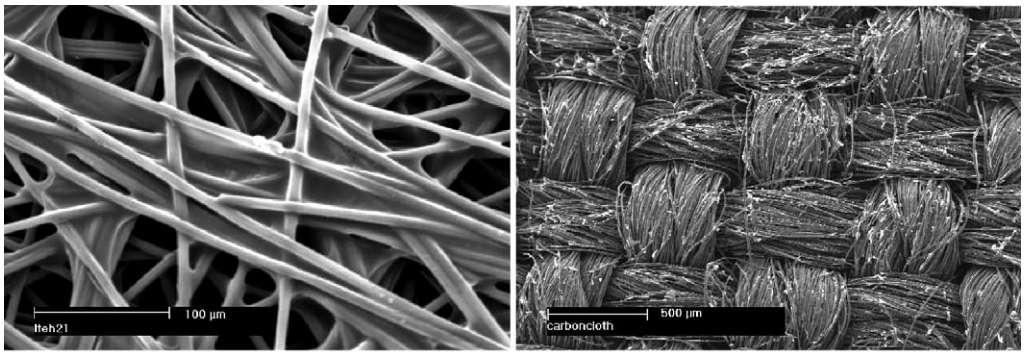

(a) (b)

Fig. 9. SEM micrographs of: (a) carbon paper, and (b) carbon cloth.

surface wettability. Therefore, it is insightful to compare the differences in the pore structure of carbon paper and carbon cloth. Fig. 9 shows SEM micrographs of these two substrates. Clearly, carbon cloth has more regularly distributed pores, whereas carbon paper is more of a random porous medium. This difference in the pore size distribution gives rise to the fact that CO_2 bubbles emerge more uniformly from the carbon cloth than carbon paper.

The bubble detachment diameter is strongly correlated with surface wettability. Consider a bubble growing and detaching from a single pore of known diameter, d_p, and surface contact angle of θ. Assuming, as was indicated in experimental observations, that the bubble detachment process is dominated by buoyancy and surface tension effects, the force balance predicts that the diameter of the bubble at detachment, d_b, is [21]:

$$d_b = \left(\frac{4 d_p \sigma \sin\theta}{g(\rho_l - \rho_g)} \right)^{1/3} \quad (1)$$

where g is gravity, ρ_l and ρ_g are the densities of the liquid and the gas respectively, σ the liquid/gas interfacial tension, and d_p the backing pore size. With the typical pore size of 10 μm for both carbon paper and carbon cloth [22], Eq. (1) calculates the bubble detachment diameter of 0.68 mm for the hydrophobic carbon paper (e.g. $\theta = 100^\circ$) and 0.38 mm for the hydrophilic carbon cloth (e.g. $\theta = 10^\circ$). These theoretical estimates are consistent with experimental observations.

3.3. Cathode flooding visualization

Water management to avoid cathode flooding is also an important issue in DMFC. The electrochemical reaction occurring on the cathode side of DMFC is given by:

$$\tfrac{3}{2}O_2 + 6H^+ + 6e^- \rightarrow 3H_2O$$

Water is produced by the oxygen reduction reaction as well as transported from the aqueous anode due to diffusion and electro-osmotic drag. Typically, the DMFC cathode experiences severe flooding which could degrade its performance significantly. Parameters governing water management include the humidity of the inlet air, stoichiometry (or volumetric flow rate), current density, temperature, and membrane water transport properties such as the diffusion coefficient and electro-osmotic drag coefficient.

Fig. 10 displays an image of water flooding on carbon paper with non-humidified air preheated to 85 °C and fed at a volumetric flow rate of 68 ml/min. The cell current density was 100 mA/cm^2. It is shown in Fig. 10 that water droplets are attached on the surface of the carbon paper due to its decreased hydrophobicity at elevated temperatures. It was observed that while the droplets grows slowly, the cell voltage drops gradually when the current density is fixed. It was also observed that the droplets will not disappear until either the current density is adjusted to a lower value or a higher volume flow rate is used.

Fig. 11 shows an image of flooding on the single-side ELAT carbon cloth (C-MEA) with non-humidified air preheated to 85 °C. It is seen from Fig. 11 that the surface of carbon cloth is nearly free of liquid droplets due to its higher hydrophobicity, but liquid droplets or 'sweating' can be found in contact corners between the stainless steel rib and carbon cloth. This is because the rib surface is rather hydrophilic. Interestingly, it appears that sweating inside corners between the ribs and carbon cloth gas diffusion layer

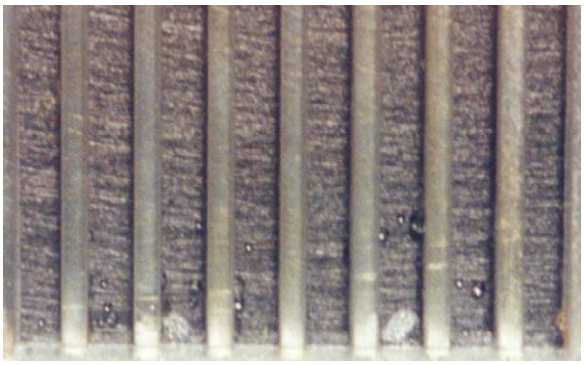

Fig. 10. Cathode flooding on Toray carbon paper for 2 M MeOH feed (20.8 ml/min and 0 psig) and non-humidified air (68 ml/min and 1 psig) at 100 mA/cm^2 and 85 °C.

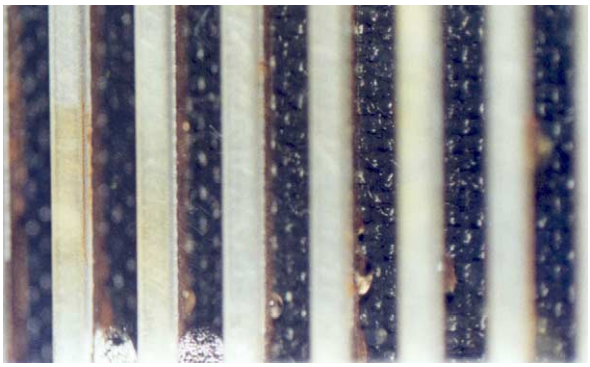

Fig. 11. Cathode flooding on single-sided ELAT carbon cloth for 2 M MeOH feed (20.8 ml/min and 0 psig) and non-humidified air (161 ml/min and 1 psig) at 60 mA/cm^2 and 85 °C.

occurs at a rather low current density of 60 mA/cm^2 and a high air flow rate of 161 ml/min. In comparison, no such sweating is seen between the stainless steel ribs and carbon paper GDL at a higher current density of 100 mA/cm^2 and a lower airflow rate of 68 ml/min (see Fig. 10).

4. Conclusions

A transparent direct methanol fuel cell was designed to enable simultaneous flow visualization and electrochemical characterization. Two types of MEAs using Nafion® 112, one made in-house with Toray carbon paper and the other commercially obtained with carbon cloth, have been investigated for their polarization characteristics at different methanol concentrations. The transparent fuel cell is shown to reach a power output of 93 mW/cm^2 at 0.302 V using in-house MEA with 2 M methanol solution and preheated temperature of 85 °C. It is pointed out that increasing the mass transport resistance of the backing layer by adding a low-permeability microporous layer provides an effective means of reducing methanol crossover. The advantage of this new strategy is to allow the use of: (1) thinner membranes, thereby lowering the cell ohmic loss, and (2) higher methanol concentration fuel, thus substantially reducing the size of the fuel tank for portable systems.

Visualization of bubble dynamics on the anode side revealed drastic differences between the two types of backing layers. For the hydrophobic carbon paper, it is found that bubbles nucleate at certain locations and form large and discrete gas slugs in the channel. Bubble detachment from the backing layer is significantly retarded by strong surface tension. For the hydrophilic, untreated carbon cloth, it is shown that bubbles are produced uniformly and with smaller size. In addition, bubbles are detached more easily by buoyancy force upon reaching ∼0.5 mm in diameter. It is thus concluded that a backing layer having uniform pore distribution and strong hydrophilicity will facilitate gas management in the anode.

Flow visualization of cathode flooding indicates that more water droplets appear upon the carbon paper GDL surface than upon the single-side ELAT GDL, due mainly to higher hydrophobicity of the latter material at elevated temperatures. However, the carbon cloth GDL yields more sweating in the corners between the GDL and hydrophilic stainless steel ribs.

Overall, the experiments helped to acquire a quantitative understanding of the intricate interactions between two-phase transport processes and material properties in DMFC. Such a basic understanding is indispensable for DMFC design and optimization.

Acknowledgements

This work was supported by DARPA Microsystem Technology Office (MTO) under contract no. DAAH01-1-R001. The first author would also like to acknowledge Dr. Chan Lim of ECEC at Penn State University for his help and useful discussions on the experiments.

References

[1] S.R. Narayanan, H. Frank, B. Jeffries-Nakamura, M. Smart, W. Chun, G. Halpert, J. Kosek, C. Cropley, in: S. Gottesfeld, G. Halpert, A. Landgrebe (Eds.), Proton Conducting Membrane Fuel Cells I, PV 95-23, The Electrochemical Society Proceedings Series, Pennington, NJ, 1995, p. 278.
[2] A. Kuver, W. Vielstich, J. Power Sources 74 (1998) 211–218.
[3] X. Ren, T.E. Springer, S. Gottesfeld, J. Electrochem. Soc. 147 (2000) 92–98.
[4] L.J. Hobson, H. Ozu, M. Yamaguchi, S. Hayase, J. Electrochem. Soc. 148 (2001) A1185–A1190.
[5] S.C. Thomas, X. Ren, S. Gottesfeld, P. Zelenay, Electrochim. Acta 47 (2002) 3741–3748.
[6] B. Gurau, E.S. Smotkin, J. Power Sources 112 (2002) 339–352.
[7] A.K. Shukla, C.L. Jackson, K. Scott, R.K. Raman, Electrochim. Acta 47 (2002) 3401–3407.
[8] M.M. Mench, C.Y. Wang, J. Electrochem. Soc. 150 (2003) A79–A85.
[9] C. Lamy, J.-M. Leger, S. Srinivasan, in: J.O'M. Bokris, R.E. White, B.E. Conway (Eds.), Modern Aspects of Electrochemistry, Kluwer/Plenum Publishers, New York, 2001, p. 53.
[10] A.S. Arico, S. Srinivasan, V. Antonucci, Fuel Cells 1 (2001) 133–161.
[11] T.I. Valdez, S.R. Narayanan, in: S. Gottesfeld, T.F. Fuller, G. Halpet (Eds.), Proton Conducting Membrane Fuel Cells II, PV98-27, The Electrochemical Society Proceeding Series, Pennington, NJ, 1998, p. 380.
[12] A. Heinzel, V.M. Barragan, J. Power Sources 84 (1999) 70–74.
[13] X. Ren, P. Zelenay, S. Thomas, J. Davey, S. Gottesfeld, J. Power Sources 86 (2000) 111–116.
[14] R. Apgyropoulos, K. Scott, W.M. Taama, Electrochim. Acta 44 (1999) 3575–3584.
[15] R. Apgyropoulos, K. Scott, W.M. Taama, J. Appl. Electrochem. 29 (1999) 663–671.
[16] T.E. Springer, T.A. Zawodzinski, S. Gottesfeld, J. Electrochem. Soc. 138 (1991) 2334–2341.
[17] C.Y. Wang, in: W. Vielstich, A. Lamm, H.A. Gasteiger (Eds.), Handbook of Fuel Cells—Fundamental, Technology and Application, vol. 3, Wiley, 2003, Chapter 29, p. 337.

[18] K. Tüber, D. Pócza, C. Hebling, J. Power Sources 124 (2003) 403–414.
[19] C. Lim, C.Y. Wang, J. Power Sources 113 (2003) 145–150.
[20] G.Q. Lu, C.Y. Wang, T.J. Yen, X. Zhang, Electrochim. Acta 49 (2004) 821–828.
[21] G.B. Wallis, One Dimensional Two-phase Flow, McGraw-Hill, New York, 1969.
[22] M.F. Mathias, J. Roth, J. Fleming, W. Lehnert, in: W. Vielstich, A. Lamm, H.A. Gasteiger (Eds.), Handbook of Fuel Cells—Fundamental, Technology and Application, vol. 3, Wiley, 2003, p. 517.